






RESEARCH ARTICLE

Position-specific carbon isotope analysis of serine by gas chromatography/Orbitrap mass spectrometry, and an application to plant metabolism

Elise B. Wilkes¹  | Alex L. Sessions¹  | Sarah S. Zeichner¹  | Brooke Dallas¹  | Brian Schubert² | A. Hope Jahren³  | John M. Eiler¹

¹Division of Geological and Planetary Sciences, Caltech, Pasadena, CA, USA

²School of Geosciences, University of Louisiana at Lafayette, Lafayette, LA, USA

³Centre for Earth Evolution and Dynamics, University of Oslo, Oslo, Norway

Correspondence

E. B. Wilkes, Division of Geological and Planetary Sciences, Caltech, Pasadena, CA, USA.

Email: ebwilkes@caltech.edu

Funding information

Agouron Institute, Grant/Award Number: AI-F-GB54.19.2; Caltech Center for Environmental and Microbial Interactions; Department of Energy, Grant/Award Number: DE-SC0016561; NASA Astrobiology Institute, Grant/Award Number: 80NSSC18M094; National Science Foundation Geobiology, Grant/Award Number: EAR-1921330; Research Council of Norway, Grant/Award Number: 223272; Simons Foundation

Rationale: Position-specific $^{13}\text{C}/^{12}\text{C}$ ratios within amino acids remain largely unexplored in environmental samples due to methodological limitations. We hypothesized that natural-abundance isotope patterns in serine may serve as a proxy for plant metabolic fluxes including photorespiration. Here we describe an Orbitrap method optimized for the position-specific carbon isotope analysis of serine to test our hypothesis and discuss the generalizability of this method to other amino acids.

Methods: Position-specific carbon isotope ratios of serine were measured using a Thermo Scientific™ Q Exactive™ GC Orbitrap™. Amino acids were hydrolyzed from *Arabidopsis* biomass, purified from potential matrix interferences, and derivatized alongside standards. Derivatized serine (*N,O*-bis(trifluoroacetyl)methyl ester) was isolated using gas chromatography, trapped in a reservoir, and purged into the electron ionization source over tens of minutes, producing fragment ions containing different combinations of atoms from the serine-derivative molecule. The $^{13}\text{C}/^{12}\text{C}$ ratios of fragments with monoisotopic masses of 110.0217, 138.0166, and 165.0037 Da were monitored in the mass analyzer and used to calculate position-specific $\delta^{13}\text{C}$ values relative to a working standard.

Results: This methodology constrains position-specific $\delta^{13}\text{C}$ values for nanomole amounts of serine isolated from chemically complex mixtures. The $\delta^{13}\text{C}$ values of fragment ions of serine were characterized with $\leq 1\%$ precisions, leading to propagated standard errors of 0.7–5‰ for each carbon position. Position-specific $\delta^{13}\text{C}$ values differed by up to $ca\ 28 \pm 5\%$ between serine molecules hydrolyzed from plants grown under contrasting $p\text{CO}_2$, selected to promote different fluxes through photosynthesis and photorespiration. The method was validated using pure serine standards characterized offline.

Conclusions: This study presents the first Orbitrap-based measurements of natural-abundance, position-specific carbon isotope variation in an amino acid isolated from a biological matrix. We present a method for the precise characterization of isotope ratios in serine and propose applications probing metabolism in plants. We discuss the potential for extending these approaches to other amino acids, paving the way for novel applications.

1 | INTRODUCTION

Carbon isotope analysis of amino acids is well established in biogeochemical and ecological research, providing insights into the origins and flow of carbon in environmental systems, diet and food web dynamics, biosynthetic pathways, and metabolism.^{1–5} Such compound-specific analyses typically provide the average isotopic composition of all the carbon atoms in an amino acid due to conversion of the analyte into CO₂ for isotope ratio mass spectrometry (IRMS). However, isotopic fractionations that occur as chemical bonds are made or broken often manifest as isotopic differences between structurally non-equivalent atomic positions in molecules.^{6–9} These processes promote non-uniform isotopic patterns *within* amino acids that may serve as more selective fingerprints of various fractionating processes.

Intramolecular carbon isotope fractionations have been observed in multiple studies of amino acids,^{10–17} and theoretical, non-uniform distributions of ¹³C/¹²C have been predicted.^{18,19} Thus, position-specific isotope analysis (PSIA) of amino acids should add an additional layer of information, specificity, and interpretive power for biogeochemical and ecological studies. These natural variations represent untapped opportunities to develop new isotopic proxies.

Amino acid PSIA has been achieved previously by a range of methodologies, including isotopic nuclear magnetic resonance (NMR) spectroscopy of intact molecules, and IRMS coupled to online or offline chemical and/or thermal degradation (for reviews, see Refs ^{20–22}). Most prior amino acid PSIA studies have targeted pre-purified analytes, purchased commercially – reflecting the challenges of isolating amino acids from natural samples in large enough quantities or with sufficient purity for existing measurement strategies. For example, constraining the intramolecular distribution of ¹³C in amino acids using ¹H NMR or ¹³C NMR requires >0.05 or 1 mmol of pure analyte, respectively.^{15,23} The relatively few PSIA studies of amino acids from biological samples have used degradative techniques, producing CO₂ from the carboxyl (C-1) position of amino acids via reaction with ninhydrin.^{10,13,16,17} However, these techniques require lengthy offline preparation²⁴ (although see also recent improvements^{12,13}), and typically target a single carbon position.

High-resolution mass spectrometry provides an alternative path for PSIA of amino acids, as has been illustrated using the Thermo Scientific™ Q Exactive™ GC and HF Orbitrap™ platforms.^{11,14,25,26} Analytes are fragmented in the ion source and can be subjected to additional fragmentation in a collision cell if needed. The resulting fragment ions retain structural information and may sample different combinations of atoms from the original molecule. It is therefore possible to constrain position-specific isotopic variations within a molecule by precisely measuring ¹³C/¹²C ratios of complementary fragment ions. This strategy is enabled by the high mass-resolving power of the Orbitrap family of analyzers. Fragments of derivatized amino acids typically have masses falling below *ca* 200 Da and require a mass resolution of up to *ca* 70 000 to observe their isotopologues simultaneously and distinguish near isobars – i.e. substitutions by ¹³C, ²H, ¹⁵N, or hydrogen adducts. Orbitrap mass analyzers within the Q

Exactive platforms surpass these requirements, achieving resolutions of at least 120 000 ($M/\Delta M$, where M is the mass and ΔM is a peak's full width at half maximum) in the mass range of interest. In principle, the Q Exactive platforms also permit online separation of molecules from complex mixtures because they can be coupled to gas chromatography (GC) or liquid chromatography (LC) systems.

Orbitrap-based approaches have been investigated for amino acid PSIA in several prior published reports: Neubauer et al¹⁴ characterized the $\delta^{13}\text{C}$ values of three separate carbon positions and the average for the remaining two positions in pure methionine standards; Eiler et al²⁶ characterized the C-1 position of pure alanine; and Chimiak et al¹¹ constrained all three carbon positions in alanine extracted from meteorite samples. Nevertheless, these techniques are still in early stages of development with limited application thus far to samples of interest to biogeochemists and ecologists. For example, it is challenging to isolate methionine from natural samples,²⁷ and the measurements of meteoritic alanine had propagated uncertainties for individual carbon positions that could not differentiate natural variations on Earth.

Serine (C₃H₇NO₃) isolated from plant samples presents an opportunity to optimize Orbitrap-based amino acid PSIA and demonstrate the applicability of such a method to amino acids derived from biologic proteins, a common sample type for biogeochemical and ecological applications. Serine is an abundant proteinogenic amino acid that plays a fundamental role in carbon and nitrogen metabolism. It has three structurally distinct carbon positions – the carboxyl carbon (C-1), the amino carbon (C-2), and the hydroxymethyl side-chain carbon (C-3). Serine has multiple metabolic sources in plants (Figure 1). Serine is synthesized along the photorespiratory pathway from two molecules of glycine via the reactions of glycine decarboxylase (GDC) and serine hydroxymethyltransferase (SHMT; Figure 1A). One molecule of glycine is decarboxylated by GDC, releasing the C-1 of glycine as CO₂; the former C-2 of glycine binds to tetrahydrofolate (THF) to form methylene-THF.²⁸ Then, SHMT catalyzes the reaction of methylene-THF with a second molecule of glycine to form serine (C-3; Figure 1A). Plant serine is also synthesized from 3-phosphoglycerate, an intermediate of glycolysis and the Calvin cycle, via the glycerate and phosphorylated pathways, with either hydroxypyruvate or 3-phosphoserine as the direct precursor to serine (Figures 1B and 1C).^{29–32}

We hypothesized that isotope effects associated with enzymes along serine's biosynthetic pathways in plants (Figure 1) would lead to measurable, position-specific differences in serine that could record useful signatures of metabolic fluxes. In particular, changes in fluxes through the photorespiratory salvage pathway versus through photosynthesis (and downstream glycolysis) would have different intramolecular isotopic consequences. Here, we apply GC Orbitrap mass spectrometry to PSIA of serine hydrolyzed from the model angiosperm *Arabidopsis thaliana* and delivered to the mass spectrometer following online chromatographic separation and peak capture. We use these samples to demonstrate performance and sensitivity of the method. Our preliminary measurements suggest that serine PSIA could serve as a position-specific isotopic proxy for

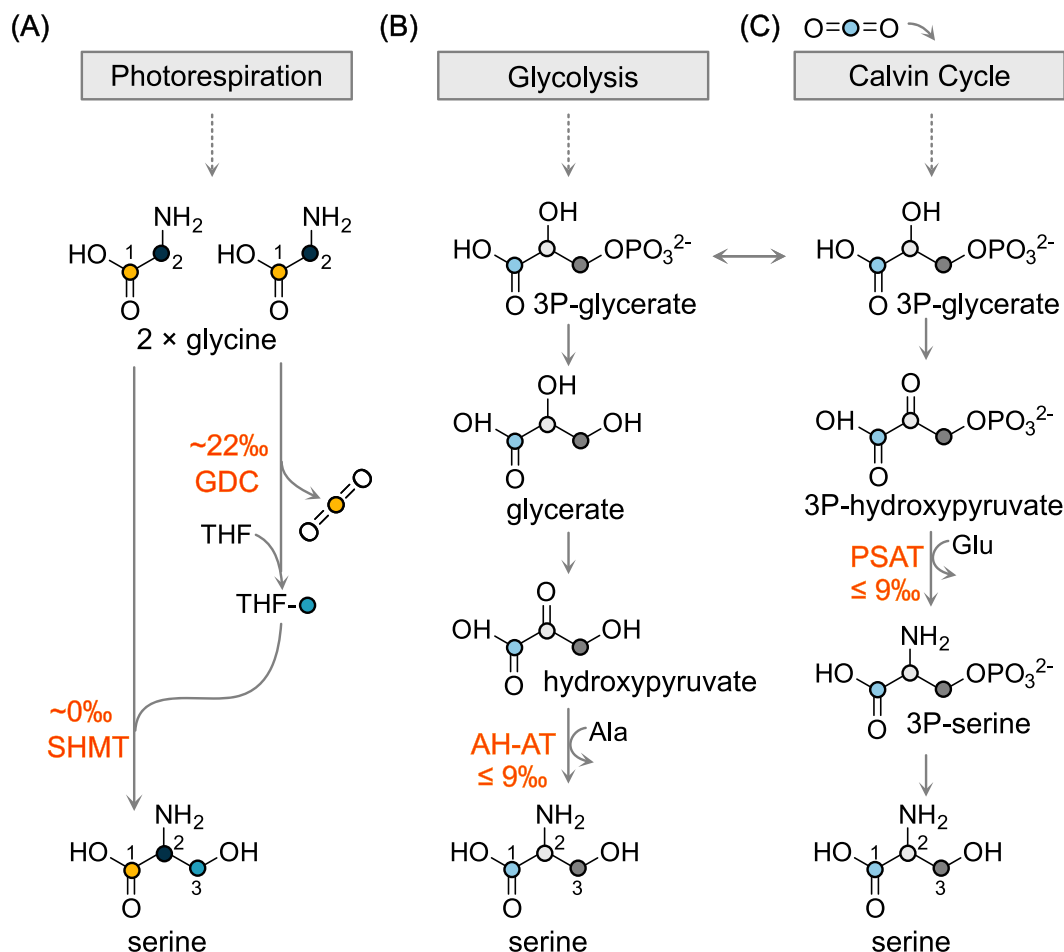


FIGURE 1 The three pathways of serine biosynthesis in C₃ plants. Serine is synthesized from intermediates of photorespiration, glycolysis, and the Calvin cycle via (A) the photorespiratory salvage pathway, (B) the glycerate pathway, and (C) the phosphorylated pathway. Carbon atoms are tracked through each pathway with colored circles. GDC, glycine decarboxylase; SHMT, serine hydroxymethyltransferase; AH-AT, alanine hydroxypyruvate aminotransferase; PSAT, 3-phosphoserine aminotransferase; THF, tetrahydrofolate. Likely kinetic isotope effects associated with each enzyme are discussed in Section 3.3 and indicated in orange [Color figure can be viewed at wileyonlinelibrary.com]

changes in plant metabolic fluxes including photorespiration. Finally, we discuss prospects for generalizing this approach to other amino acids and environmental samples.

2 | EXPERIMENTAL

2.1 | Method overview

Peptide-bound amino acids were liberated from dried plant samples by acid hydrolysis, followed by solvent extraction and ion exchange to remove lipophilic components and salts, respectively. The acid hydrolysates were then derivatized alongside pure amino acid standards through sequential methylation and trifluoroacetylation steps. The amino acids were separated by GC, and the target analyte was directed into a 10 or 25 mL reservoir, enabling its isolation and gradual release into the ion source of the Orbitrap mass spectrometer. Following ionization, selected fragment ions were admitted through a quadrupole mass filter into a curved linear trap and then the Orbitrap

mass analyzer. Ions were injected into the mass analyzer and then observed for brief periods (“scans”), repeated many times for up to 50 min. These repeated observations in the Orbitrap were used to calculate the ¹³C/¹²C ratio of each fragment of interest. Alternating sample and standard injections (“acquisitions”) were used to calculate δ¹³C values for each fragment ion, and multiple sample–standard comparisons were averaged. In turn, these average δ¹³C values of fragment ions were used to calculate the δ¹³C values for atomic positions within the parent molecule relative to a serine working standard (see Section 2.7).

2.2 | Working standards

Working standards were prepared to achieve four goals: (1) to assess the measurement accuracy, precision, and sensitivity of the method, (2) to serve as reference standards for Orbitrap isotope ratio measurements, (3) to identify the serine carbon positions inherited by fragment ions, and (4) to optimize Orbitrap measurement parameters.

L-Serine (lot no. BCBS0964V, certified purity $\geq 99.5\%$, BioUltra; $C_3H_7NO_3$) was purchased from Sigma-Aldrich (St Louis, MO, USA). Approximately 2 g was dissolved in Milli-Q water, then dripped into liquid nitrogen, freeze-dried, and ground to a homogenous powder using a glass stir rod. The resulting serine working standard is called SERCO, with the "0" in the name indicating that no isotopic label was added. L-Serine-1- ^{13}C (99 atom% ^{13}C label at C-1) was purchased from Sigma-Aldrich; 0.97 mg of the label was combined with 2425.9 mg of the unlabeled BioUltra serine and homogenized as above. The resulting mixture is SERC1, indicating that the C-1 carbon position has been ^{13}C -enriched. Separately, 0.49 mg of L-serine-2- ^{13}C (99 atom% ^{13}C at C-2; Sigma-Aldrich) was combined with 2271.6 mg of BioUltra serine and homogenized to produce SERC2. Additional batches of L-serine (lot no. BCBS0964V, $\geq 99.5\%$; and lot no. 110M0205V, $\geq 98.5\%$; purchased from Sigma-Aldrich) lacking ^{13}C label were used without further homogenization or purification (hereafter called LotBCB and Lot110, respectively).

The molecular-average (C-1 + C-2 + C-3) carbon isotopic compositions of SERCO, SERC1, and SERC2 were measured at Caltech via an EA IsoLink™ combustion elemental analyzer system interfaced to a Delta V Plus isotope ratio mass spectrometer (EA/IRMS, Thermo Scientific, Bremen, Germany), calibrated against international reference materials (USGS-44, USGS-45 glycines; USGS-73, USGS-74 valines; caffeine; NIST-8542 sucrose). Lot110 and LotBCB serines were also measured using this EA/IRMS system, calibrated against NIST-8542 sucrose and a laboratory working standard of urea. Molecular-average carbon isotopic compositions of trifluoroacetylmethyl ester derivatives of the Lot110 and LotBCB standards (Section 2.4) were measured at Caltech by GC/C/IRMS (Thermo Finnigan™ TraceGC Ultra interfaced to a DELTA^{plus} XP via a GC/C III combustion interface) using a ZB-5ms column (30 m \times 0.25 mm ID, 0.25 μ m film thickness). The oven program was: 50°C (hold 1 min), ramp to 120°C at 3°C/min (hold 7 min).

The carboxyl carbons (C-1) of the SERCO, SERC1, and SERC2 reference materials were isotopically characterized at Tokyo Tech by decarboxylating the standards with ninhydrin³³ and measuring the liberated CO₂. Approximately 1 mg of the reference material was added to a gas-tight vial flushed with helium, then heated with acidic ninhydrin solution (3 h, 100°C). The resulting CO₂ was analyzed using GC coupled with an IRMS instrument (Delta^{plus}XP, Thermo Fisher Scientific) via a GC Combustion III interface (Thermo Fisher Scientific). Samples were injected in split mode at 250°C. An HP-PLOT-Q (30 m \times 0.32 mm ID, 10 μ m film thickness; Varian, CA, USA) column was used with high-purity helium as carrier gas at 1.5 mL/min. The GC oven temperature was held constant at 50°C. Isotopic standardization was accomplished by injecting CO₂ calibrated against NIST natural gas standard NGS-2.

2.3 | Plant sample preparation

A. *thaliana* Col-0 plants were previously grown from seed to maturity in controlled growth chambers (122 cm \times 91 cm \times 46 cm) under

multiple CO₂ levels ranging from 97 to 2255 ppmv in order to test the effect of pCO_2 level on carbon isotope discrimination.^{34,35} Within these experiments, the ambient gas composition (pCO_2 , $\delta^{13}C_{VPDB}$ value), temperature, relative humidity, and soil moisture were maintained and monitored using established protocols.^{36,37} A subset of these samples, representing dried, powdered samples of above-ground tissues grown under highly elevated (2255 \pm 148 ppmv), elevated (733 \pm 18 ppmv), or subambient (322 \pm 4 ppmv) pCO_2 levels and ambient pO_2 (ca 21%) were selected for the present study to include conditions that should foster different balances of photorespiration (O₂ fixation) and photosynthesis (CO₂ fixation), although these fluxes were not quantified. A total of 10–15 mg of the powdered samples, combined from two or three biological replicates, was weighed into 40 mL VOA vials with Teflon-lined caps and then subjected to acid hydrolysis (6 N HCl, 16 h, 108°C, argon headspace), with conditions selected to optimize recovery of serine (reviewed in Silverman et al.³⁸). This type of acid hydrolysis has been shown to have little impact on serine's carbon isotopic composition in prior studies,^{39,40} and was confirmed for our specific protocol by subjecting an external standard containing SERCO to the entire preparatory workflow. The 6 N HCl used for the hydrolysis was first bubbled with argon, then 4 mL was added to each sample, and the sample vials were flushed with argon and heated in a digital block heater.

Acid hydrolysates were diluted with 2 mL of Milli-Q water, bringing the total volume in each vial to 6 mL, then washed via liquid/liquid extraction with two bed volumes of hexanes and dichloromethane (6:5, v/v) to remove lipophilic components.⁴¹ The aqueous phase was removed to a clean 40 mL VOA vial and dried on a 100°C hot plate under a stream of N₂, re-dissolved in 2 mL of 0.1 N HCl, then desalted by cation-exchange chromatography using analytical-grade resin (Dowex AG 50W-X8; 100–200 mesh, H⁺ form) from Bio-Rad Laboratories (Tokyo, Japan) in glass pipette columns plugged with quartz wool. The resin was washed with three bed volumes each of 1 N HCl, Milli-Q water, 1 N NaOH, and water, then the sample was loaded and washed with Milli-Q water.⁴¹ Amino acids were eluted into a clean vial with 10 wt% NH₃ aqueous solution and dried under N₂.

2.4 | Derivatization

Desalted acid hydrolysates were transferred quantitatively in Milli-Q water to 2 mL GC vials and dried under N₂. Reference standards (1 mg) were weighed into separate 2 mL GC vials and derivatized in parallel with the plant hydrolysates, using the same batches of reagents. Anhydrous methanol (100 μ L, >99.9% purity, Macron Fine Chemicals) was added to each vial and placed on ice; acetyl chloride (25 μ L; $\geq 99.0\%$, Sigma Aldrich) was added dropwise. Vials were capped and heated at 70°C for 1 h.⁴² The resulting methyl esters were dried under a gentle stream of N₂ at room temperature. Dichloromethane (DCM; 2 \times 100 μ L) was added to the vials for azeotropic drying, then carefully evaporated under N₂. The resulting amino acid methyl esters were trifluoroacetylated by transferring

250 μL of ethyl acetate to each vial, followed by 50 μL of trifluoroacetic anhydride (>99% purity, Sigma Aldrich). Vials were capped tightly and heated at 110°C for 10 min. Excess reagent was removed under N_2 at room temperature. DCM (1 \times 100 μL) was added to the vials, then evaporated in a gentle stream of N_2 .

The full derivatization protocol yielded *N,O*-bis(trifluoroacetyl) serine methyl ester (monoisotopic mass 311.0228 Da) and other amino acid trifluoroacetyl methyl esters (TFA-ME). Derivatives were brought up in 1 mL of hexane, and tenfold serial dilutions were prepared in hexane for GC injections.

2.5 | Instrumentation

A schematic representation of the Q Exactive Orbitrap mass spectrometer used in this study is shown in Figure 2. This platform employed a Thermo Scientific TRACE™ 1310 GC equipped with split/splitless injector. Peaks eluting directly off the GC column have been explored for isotope analysis, illustrating that the achievable precision is limited by the number of ions (10^4 – 10^5) observed per scan in the Orbitrap and the width of the chromatographic peak (in time).⁴³ Our application therefore required a distinct instrumental setup to achieve the desired precision (i.e. $\leq 1\%$). We modified the system to spread out chromatographic peaks and increase the number of measured ions by adding two 4-port, 2-position Valco™ switching valves as described elsewhere.²⁶ The modification enabled us to direct the serine GC peak into a reservoir, from which it slowly and continuously eluted into the Orbitrap enabling observation for repeated scans over a period of up to 50 min. The remaining GC effluent (and thus all other amino acids) is sent to waste, rather than to the reservoir and Orbitrap. Here, we used a Silco-coated stainless steel reservoir (10 or 25 cm^3 ; SilcoTek, Bellefonte, PA, USA) in place of a glass reservoir to minimize adsorptive losses.

Amino acid samples were injected in splitless mode at 250°C with a 4 mm ID deactivated glass liner. Chromatographic separation was carried out on a 30 m \times 0.25 mm ID capillary column (TG-5SIL MS, 0.25 μm film thickness; Thermo Scientific) with helium carrier gas at 1.4 or 1.5 mL/min. Orbitrap experiments that exclusively targeted pure serine standards used oven temperature programs of 50 to 120°C at 7°C/min or 50 to 90°C at 15°C/min (hold isothermal). For studies including plant samples, both the plants and standards were characterized under identical conditions by ramping the oven from 50 to 90°C at 1°C/min and holding isothermal at 90°C until serine had finished eluting out of the GC system. For acquisitions making use of a peak-broadening reservoir, the size of the reservoir dictated the isothermal hold time required for serine to completely elute. An additional oven ramp from 90 to 120°C was added to the end of acquisitions, where applicable, to allow later-eluting amino acids to clear the column.

Analytes were transferred from the GC column, or from the peak-broadening reservoir downstream of the column, into the electron ionization (EI) source (70 eV; Thermo Scientific™ ExtractaBrite™) via a 250°C capillary transfer line. Selected ion species were admitted through the advanced quadrupole selector (AQS) with a relatively narrow isolation window of 7 or 8 Da to minimize observation of non-serine ions that could exacerbate space-charge effects and spectral noise. Even narrower isolation windows of less than 7 Da were not attempted in this study because ion transmission through the AQS is known to vary across the selected mass range and could fractionate isotopologues if smaller AQS windows are used (see Figure 6 in Eiler et al²⁶). Ion species accumulated in a curved linear trap (C-trap) to numbers controlled by the automatic gain control (AGC) algorithm. Ions were then transferred from the C-trap to the Orbitrap mass analyzer. The Orbitrap operates by trapping moving ions in an electrostatic field under ultrahigh vacuum.⁴⁴ Ions oscillate along a central electrode with frequencies proportional to $(m/z)^{1/2}$. Ion currents as a function of time are recorded by image current

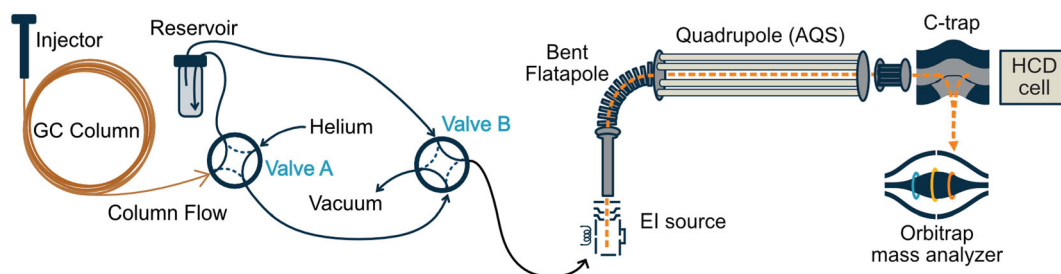


FIGURE 2 Schematic representation of the Thermo Scientific Q Exactive GC/Orbitrap with custom modifications used in this study. A commercially available Thermo Scientific trace 1310 gas chromatograph was modified to include valves A and B, which enable four distinct run configurations (described in detail in Eiler et al²⁶). The configuration shown transfers compounds eluting off the GC column into an inert, passivated stainless steel reservoir which serves as an exponential dilution flask to broaden the chromatographic peak. The reservoir is continuously purged into an EI source in the displayed configuration, but can also be directed to a waste stream (vacuum) or bypassed altogether by turning valve A. Analytes are ionized and fragmented in the source and move through the bent flatapole into the AQS which is used to isolate ions falling within designated mass ranges. Ions accumulate in the curved linear trap (C-trap), to levels specified by the AGC target value, and are collisionally cooled. Packets of ions are then injected into the Orbitrap mass analyzer for discrete analyses (“scans”). The Q Exactive platform also includes a higher-energy collisional dissociation (HCD) cell, which enables additional fragmentation downstream of the ion source, but this feature is not used in our method for serine [Color figure can be viewed at [wileyonlinelibrary.com](https://onlinelibrary.wiley.com)]

detection, and the frequencies are recovered by fast Fourier transform of that time-varying signal, then converted into a mass spectrum.^{26,45,46}

The maximum injection time allowed per scan was 3000 ms. Data from multiple microscans were never averaged within the instrument software. AQS isolation windows (scan mass ranges) for precise isotopic measurements were 107–114, 134.5–142.5, or 162–169 *m/z*. A nominal mass resolution ($M/\Delta M$) of 120 000 was used across all analyses (full-width, half-maximum definition at 200 Da; mass resolutions at the measured masses of interest were higher, generally in the range 140 000 to 170 000). The AGC target was set to either 200 000 or 20 000 ions (see Section 2.9).

2.6 | Orbitrap data processing

FTStatistic software (Thermo Fisher Scientific) was used for extraction of signal intensities and other acquisition data from the instrument RAW files. Python (version 3.7) was used for subsequent data analysis. Extracted signals (S) were converted to ion counts (i.e. numbers of observed ions; N_{IO}) following Equation (1),²⁶ where N is the extracted peak noise, C_N is the number of charges of the Orbitrap noise band (here, uniformly taken to be 4.24 at the reference resolution, R_N , of 120 000), R is the nominal resolution, and z is the charge per ion at the mass of interest (see supporting information for additional explanation):

$$N_{IO} = (S/N)(C_N/z)(R_N/R)^{1/2} \quad (1)$$

Each acquisition contained thousands of scans reporting signals for the monoisotopic (^{12}C) fragment, the ^{13}C -substituted fragment, or both. Scans not detecting both isotopologues were discarded, as were scans with injection times equaling the maximum injection time setting. Scans in which the baseline-subtracted ^{12}C signal was <10% of the maximum, baseline-subtracted ^{12}C signal for the serine peak were also discarded. For each remaining scan, the signal for each isotopologue was converted to an ion count via Equation (1). The ion counts for each isotopologue were then summed across the entire chromatographic peak, and ^{13}R was calculated as the ratio of ion counts (Equation 2). These apparent isotope ratios were compared between sample and a standard to calculate a $\delta^{13}\text{C}$ value (Equation 3), expressed as parts per thousand (per mil, ‰) deviations from the standard.

$$^{13}\text{R} = \frac{\sum ^{13}\text{C fragment ion counts}}{\sum ^{12}\text{C fragment ion counts}} \quad (2)$$

$$\delta^{13}\text{C}_{\text{standard}} = \frac{^{13}\text{R}_{\text{sample}} - ^{13}\text{R}_{\text{standard}}}{^{13}\text{R}_{\text{standard}}} \quad (3)$$

Note that no individual scans were weighted more heavily than others when calculating isotope ratios. Weighted (following Chimiak et al¹¹)

and unweighted calculations were considered in this work, and we consistently found that our unweighted approach (Equation 2) yielded better agreement between replicate runs and more accurate $\delta^{13}\text{C}$ values for standards of known composition.

2.7 | Calculation of position-specific $\delta^{13}\text{C}$ values

Candidate fragment ions for this work were identified from the full mass spectrum of derivatized serine. A particular requirement of our approach is that the positional origin of every carbon atom in every measured fragment must be known. The possibility of ion rearrangements, multiple fragmentations, and recombination (particularly H- and CH_3 -transferring reactions) in the EI source make this task harder than it may at first sound. Moreover, to uniquely constrain N different carbon positions, we require N different measurements that sample those positions in different combinations, i.e. N linearly independent constraints. The molecular structures of candidate fragment ions were first elucidated by examining their exact masses in combination with predictions from spectral interpretation software (Mass Frontier™, Thermo Scientific), to narrow the number of candidate fragments. Next, contributions to the fragments from particular positions within the parent serine molecule or derivative groups were confirmed by isotope labeling experiments. Serine standards prepared with 10% ^{13}C label at the C-1, C-2, or C-3 atom positions, respectively, were derivatized and eluted from the GC column directly into the Orbitrap (bypassing the reservoir) to quickly assess which parent atoms were inherited by different candidate fragment ions. The presence of label was detected by monitoring the ^{13}C -substituted signal for each fragment. Parent atom inheritance was further confirmed through precise isotopic analysis of positionally labeled SERC1 and SERC2 standards (Section 3.2). We refer to the collection of all such inheritance patterns for all fragments being measured as the “inheritance matrix.”

Figure 3 shows a representative mass spectrum (50–200 *m/z*) of the serine TFA-ME derivative, including molecular structures and inherited carbon positions. We concluded that the best fragment ions for serine PSIA have monoisotopic masses of 110.0217, 138.0166, and 165.0037 Da, each with an associated ^{13}C -substituted signal (+ 1.003355 Da) that was baseline resolved. Collectively, these six fragment ions enable direct calculation of position-specific $\delta^{13}\text{C}$ values relative to a working standard for every chemically unique position in serine. An inheritance matrix was constructed that related the measured $\delta^{13}\text{C}$ values of the fragments to the positional $\delta^{13}\text{C}$ values, which can be calculated either by direct matrix algebra (Figure 3D) or by simplifying to Equations (4)–(6):

$$\delta^{13}\text{C}_{\text{C-1,standard}} = 5 \times \delta^{13}\text{C}_{165} - 4 \times \delta^{13}\text{C}_{138} \quad (4)$$

$$\delta^{13}\text{C}_{\text{C-2,standard}} = 3 \times \delta^{13}\text{C}_{110} \quad (5)$$

$$\delta^{13}\text{C}_{\text{C-3,standard}} = 4 \times \delta^{13}\text{C}_{138} - 3 \times \delta^{13}\text{C}_{110} \quad (6)$$

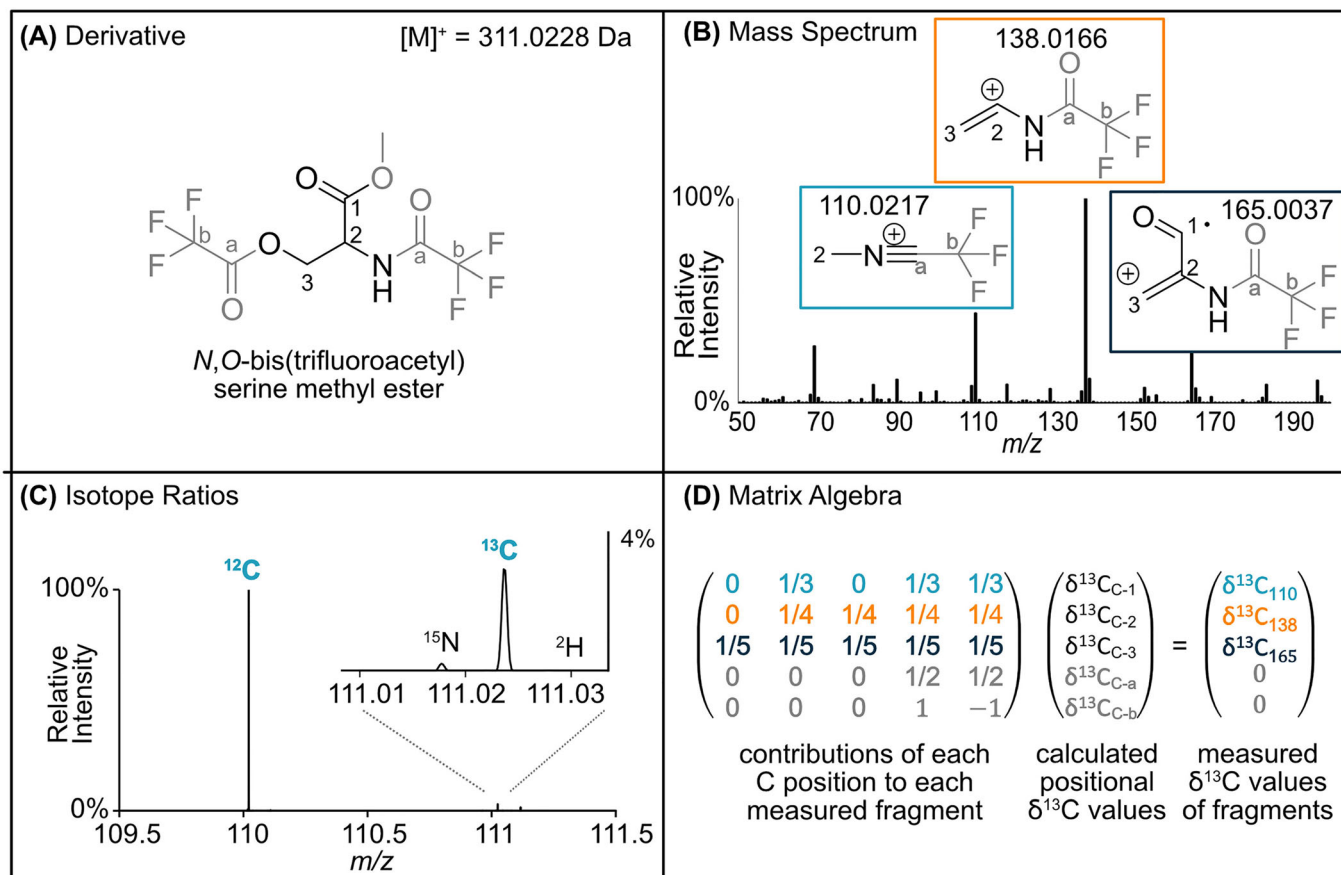


FIGURE 3 Amino acid PSIA strategy, illustrated for serine. (A) Serine is derivatized with trifluoroacetyl and methyl ester groups to increase its volatility for GC separation. Here the carbon positions within the original serine molecule are numbered, while exogenous carbons from the derivatizing reagents are lettered. (B) Representative mass spectrum of derivatized serine (70 eV EI source; 50–200 m/z scan range). Three fragment ions (including one rearrangement product) are depicted and sample different combinations of atoms from the parent serine molecule. The numbering and lettering schemes denote inherited atomic positions from the parent molecule. (C) Isotope ratios ($^{13}\text{C}/^{12}\text{C}$) are measured for each fragment by monitoring the signal intensities of each monoisotopic fragment (e.g. $[\text{C}_3\text{NH}_3\text{F}_3]^+ = 110.0217$ Da) and ^{13}C -substituted fragment ($^{13}\text{C}^{12}\text{C}_2\text{NH}_3\text{F}_3^+ = 111.0251$ Da) using a 7 or 8 Da isolation window and thousands of consecutive scans by the Orbitrap mass analyzer. (D) Measured $\delta^{13}\text{C}$ values for each fragment, expressed relative to a serine standard analyzed in the same session, are used to calculate the position-specific $\delta^{13}\text{C}$ values of the parent serine molecule via a matrix mathematically describing which carbon positions from the parent molecule were inherited by each fragment measured on the Orbitrap (the “inheritance matrix”). Rows 1–3 of the matrix algebra relate the carbon positions inherited by each fragment to $\delta^{13}\text{C}$ measurements on the Orbitrap. The fourth row of the matrix algebra describes a hypothetical fragment sampling only the derivative atoms (C-a + C-b), with each contributing half the $\delta^{13}\text{C}$ value. We assume the carbon atoms added during derivatization had identical isotopic compositions for both the sample and reference standard (thus $\delta^{13}\text{C} = 0$). The fifth row represents a final simplifying assumption that the isotopic compositions of C-a and C-b are equivalent and both equal to zero [Color figure can be viewed at wileyonlinelibrary.com]

Equations (4)–(6) assume that the exogenous carbon atoms added during derivatization had identical isotopic compositions for both the sample and reference standard and thus both had $\delta^{13}\text{C}$ values of zero (because they are referenced to the standard not VPDB). This is appropriate because the sample and standard were derivatized at the same time under identical conditions with excess reagent.⁴⁷ Another underlying assumption is that instrumental fractionations associated with the measurement impact the sample and standard identically.

In this study we did not relate calculated isotope ratios at every carbon position to the international (VPDB) scale. Doing so would require position-specific isotopic calibration of our serine working

standard to VPDB using a complementary measurement approach (e.g. isotopic NMR; see additional discussion in Section S2 of the supporting information); nevertheless, the C-1 position of SERCO standard was measured relative to VPDB using a degradative technique coupled to IRMS (ninhydrin reaction; Section 2.2). Position-specific isotope ratios of a sample ($^{13}R_{\text{sample,Orbitrap}}$) determined by Orbitrap measurements alongside a standard ($^{13}R_{\text{standard,Orbitrap}}$) are converted to other reference frames like VPDB using Equation (7), where $^{13}R_{\text{standard,true}}$ is the internationally accepted value on the VPDB scale, recovered by measuring the standard relative to another calibrated reference material:

$${}^{13}\text{R}_{\text{sample,true}} = \left(\frac{{}^{13}\text{R}_{\text{sample,Orbitrap}}}{{}^{13}\text{R}_{\text{standard,Orbitrap}}} \right) \times {}^{13}\text{R}_{\text{standard,true}} \quad (7)$$

2.8 | Error analysis and propagation

The statistical limit on precision for each acquisition was calculated as the relative shot noise error (σ_{SN}/R , Equation 8; adapted from Hayes²⁴ with the assumption that $1/{}^{12}\text{N}_{\text{IO}}$ is negligibly small) and compared to the relative acquisition error (σ_{AE}/R). The acquisition error provided a measure of how reproducibly the instrument measured isotope ratios from one scan to the next within an acquisition, dependent on the total number of scans; it was determined by calculating the ${}^{13}\text{C}/{}^{12}\text{C}$ ion count ratio for every scan within an acquisition, and then calculating the standard error of those ratios. This value was normalized by dividing by the mean isotope ratio for the acquisition.

$$\left(\frac{\sigma_{\text{SN}}}{R} \right)^2 \approx \frac{1}{{}^{13}\text{N}_{\text{IO}}} \quad (8)$$

Standard deviations (σ_{SD}) and standard errors (σ_{SE}) associated with replicate estimates of $\delta^{13}\text{C}$ values (i.e. replicate sample–standard comparisons) provided a measure of inter-acquisition variability. Additionally, shot noise errors or acquisition errors, respectively, were averaged across acquisitions. For sample–standard comparisons, average shot noise errors of samples were added in quadrature to average shot noise errors of standards. Average acquisition errors of

samples were added in quadrature to average acquisition errors of standards.

The standard error for each measured fragment was propagated for position-specific $\delta^{13}\text{C}$ values using Equations (9)–(11). Notably, these calculated uncertainties for the three serine positions are highly correlated with one another. For example, computed errors for the C-3 position of serine are correlated with those for C-1 because both calculations depend on the error associated with the 138 Da fragment, which is quadrupled when calculating position-specific uncertainties (Equations 9 and 11).

$$\sigma_{\text{C-1}} = \left((5 \times \sigma_{165})^2 + (4 \times \sigma_{138})^2 \right)^{1/2} \quad (9)$$

$$\sigma_{\text{C-2}} = 3 \times \sigma_{110} \quad (10)$$

$$\sigma_{\text{C-3}} = \left((4 \times \sigma_{138})^2 + (3 \times \sigma_{110})^2 \right)^{1/2} \quad (11)$$

2.9 | Quality evaluation

Data for every acquisition were plotted as shown in Figure 4. Acquisitions were considered successful if they had the following characteristics: (1) the masses corresponding to the ${}^{12}\text{C}$ and ${}^{13}\text{C}$ fragment ions accounted for the majority of the total ion current (TIC) for each scan window (Figure 4A; Figure S1a, supporting information; i.e. there were no obvious contaminants due to co-elution with other components of the sample matrix) and (2) the calculated ion counts were stable across an acquisition (Figure 4B; Figure S1b, supporting

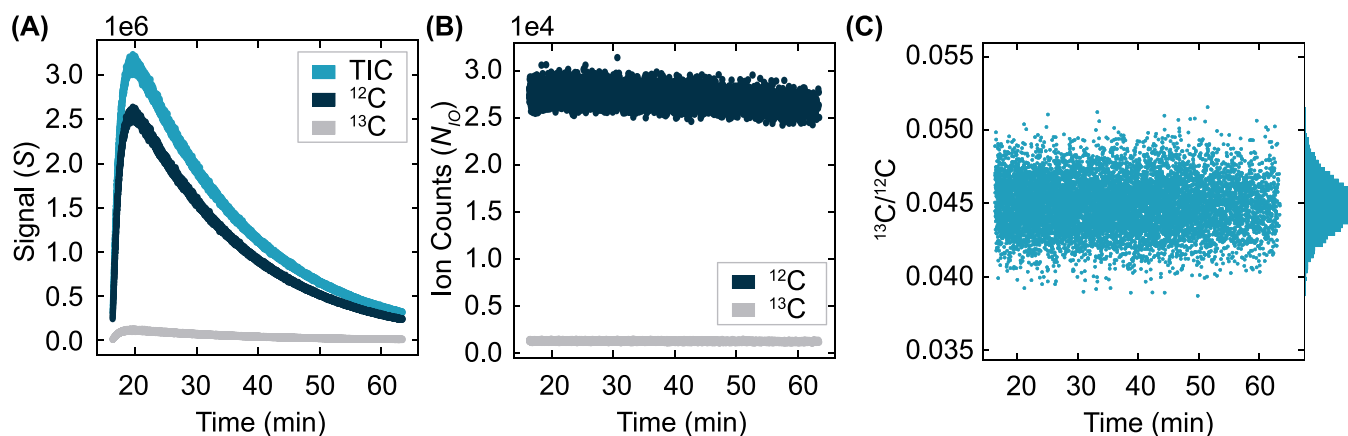


FIGURE 4 Characteristics of a measurement of a fragment ion delivered to the Orbitrap via the peak broadening reservoir. Here, the 138.0161 Da fragment (${}^{12}\text{C}$) and 139.0194 Da fragment (${}^{13}\text{C}$) of the Lot110 serine standard are shown. Data falling below 10% of the maximum 138.0161 Da peak height are discarded; see methods). (A) TIC chromatogram and selected-ion chromatograms for the ${}^{12}\text{C}$ (138.0161) and ${}^{13}\text{C}$ (139.0194) isotopologues. (B) The number of ion counts per scan (Equation 1) calculated from the signal (S) intensities in (A). Ideally these values are stable over the course of an acquisition. The difference between (A) (decreasing signal with time) versus (B) (stable ion counts) is explained mathematically by the peak noise (N) term of Equation (1), which is a time-varying parameter that also decreases with time. The Orbitrap samples the same number of ions from each interval, regardless of the TIC during that interval. (C) Isotope ratios (${}^{13}\text{R}$) calculated for each scan are stable across the acquisition and Gaussian. The ${}^{13}\text{C}$ isotope trace is expanded using a secondary y-axis in Figure S1 (supporting information) [Color figure can be viewed at wileyonlinelibrary.com]

information). Occasionally, aberrant spikes in the TIC or ion counts suggested an electronic artifact; these runs were excluded from further consideration. Isotope ratios calculated scan-by-scan also (3) appeared stable across the acquisition and were normally distributed (Figure 4C). Closer inspection of acquisition data sometimes revealed evidence of coalescence, which is an ion cloud coupling or phase locking phenomenon⁴⁸ that can cause the ¹³C-substituted fragment to apparently shift in mass and/or be subsumed by significant adjacent peaks like hydrogen adducts. Coalescence was detected by calculating an observed shift in mass between two minor species relative to their actual difference in mass; when significant (defined here as a difference exceeding 0.0001), a lower AGC target was adopted and used for both sample and standard.

2.10 | Chromatographic isolation of serine from a plant matrix

It is essential to cleanly capture serine as it elutes from the GC column, separate from other chemical species, because ions from co-eluting compounds – even if not strict isobars – can artificially depress ¹³C/¹²C ratios in the Orbitrap mass analyzer.⁴⁹ Furthermore, incomplete collection of serine can express chromatographic (vapor pressure) isotope effects.⁵⁰ Thus, we optimized the timing of valve A by initially capturing a serine standard over a relatively wide time window and sequentially narrowing the window while monitoring for changes in signal intensity and isotope ratio. We then optimized these timings further using a plant sample, monitoring the mass spectrum for contaminating masses. We also used a “reverse” peak capture experiment⁵¹ in some cases to confirm successful capture. In this type of experiment, valves A and B were configured such that the Orbitrap receives everything *except* that being diverted to the reservoir. In this case the successful, complete capture of serine was confirmed by the absence of a chromatographic peak for serine or its associated mass spectrum.

3 | RESULTS AND DISCUSSION

3.1 | Performance characteristics

Precisions of 0.2–1.0‰ (1 SE, $n = 3$ sample–standard comparisons) were achieved for $\delta^{13}\text{C}$ values measured for each fragment of derivatized serine. Acquisition errors were consistently *ca* 1.4 times shot noise errors, i.e. near the limit imposed by counting statistics. Minimum sample size requirements were influenced by the need to characterize each fragment independently – accomplished in this study by multiple, separate sample injections – and by the yield of each target fragment per injection, which was influenced by daily ion source tuning and pressure conditions. We found that a single acquisition for any chosen fragment typically required 94 ng (0.3 nmol) of derivatized serine on-column, and *ca* 3 nmol serine for the complete characterization (a minimum of 9 injections).

Approximately 50–100 μg original dry weight of *Arabidopsis* biomass was required to obtain sufficient serine for the complete characterization.

Achievable precisions were a function of the duration of Orbitrap analysis afforded by the peak-broadening reservoir (Figure S2, supporting information), as well as the GC column loading capacity (and thus the amount of derivatized serine that could be injected without co-elution of other matrix components). The best counting statistics and experimental reproducibility were achieved for the 138 and 110 Da fragments. These fragments formed most efficiently in the ion source and were the only prominent fragment ions occurring in the AQS window centered around these masses. Analyses of the 165 Da fragment were accompanied by slightly poorer precision on average. This fragment formed less efficiently under standard source tuning parameters. Furthermore, the scan range encompassed several other prominent serine-derived fragment ions and adducts, potentially contributing to space charge effects and reducing the number of targeted ion species that could be analyzed per unit time. We adopted a lower AGC target of 20 000 for this fragment in order to minimize coalescence detected between the ¹³C-substituted fragment ion and a hydrogen adduct (both with nominal mass 166 Da).

3.2 | Method validation

The accuracy of the isotopic measurements presented in this study was examined using two sets of well-characterized standards: serine prepared with different levels of ¹³C enrichment at individual carbon positions (SERC0, SERC1, and SERC2, respectively) and commercial serine (LotBCB, Lot110) with different molecular-average isotopic compositions. Isotopic differences between standards were characterized on the Orbitrap, then compared to independent constraints from complementary measurements of the same materials (Tables 1 and 2, Figure 5).

Measurement of all three fragments of SERC1 referenced to SERC0 indicated a clear ¹³C enrichment of $32 \pm 5\%$ at the C-1 position and no enrichment at the C-2 and C-3 positions. The C-2 position of SERC2 was found to have a ¹³C enrichment of $18.8 \pm 0.7\%$ relative to SERC0. These Orbitrap measurements agreed within 1 SE with expectations from independent constraints (Table 1, Figure 5), including offline measurement of C-1 by reaction with ninhydrin. The molecular-average $\delta^{13}\text{C}$ values were also measured by EA/IRMS, and the differences between SERC1 or SERC2 and SERC0 were assumed to be due to labeling at one position while the remaining carbon positions were all unchanged (Table 1, Figure 5; Section S3, supporting information).

Molecular-average $\delta^{13}\text{C}$ values of serine Lot110 and LotBCB were measured by GC/Orbitrap and agreed within uncertainty with measurements of the same materials by EA/IRMS and GC/IRMS (Table 2). The 165 Da fragment was measured in the Orbitrap because it inherits all three carbon atoms of serine (plus two reagent-derived atoms), yielding a $\delta^{13}\text{C}$ value of $15 \pm 1\%$ for Lot110,

TABLE 1 Isotopic characterization of positionally labeled serine standards used for PSIA

Analyte	Isotopic target	Strategy	Reference standard	Expected $\delta^{13}\text{C}$ (‰)	Observed $\delta^{13}\text{C}$ (‰)	σ_{SE}	<i>n</i>
SERC0	Molecule-average	EA/IRMS	VPDB		-32.22	0.02	9
	C-1	Ninhydrin	VPDB		-20.3	0.5	1
SERC1	Molecule-average	EA/IRMS	VPDB		-20.35	0.02	6
	C-1	Ninhydrin	VPDB		11.2	0.5	1
	Fragment 110	GC/Orbitrap	SERC0		-0.1	0.5	3
	Fragment 138	GC/Orbitrap	SERC0		0.2	0.3	3
	Fragment 165	GC/Orbitrap	SERC0		6.4	0.9	3
	C-1	Calculation	SERC0	32.2, ^a 36.8 ^b	31.5	4.6	
	C-2	Calculation	SERC0	0	-0.2	1.4	
	C-3	Calculation	SERC0	0	0.9	2.0	
SERC2	Molecule-average	EA/IRMS	VPDB		-26.03	0.03	6
	C-1	Ninhydrin	VPDB		-20.2	0.5	1
	Fragment 110	GC/Orbitrap	SERC0		6.3	0.2	3
	Fragment 138	GC/Orbitrap	SERC0		4.5	0.3	3
	Fragment 165	GC/Orbitrap	SERC0		2.5	1.5	3
	C-1	Calculation	SERC0	0, 0.1 ^a	-5.5	7.7	
	C-2	Calculation	SERC0	19.2 ^b	18.8	0.7	
	C-3	Calculation	SERC0	0	-0.7	1.1	

The measurement strategies (described in the text and the supporting information) used to constrain expected $\delta^{13}\text{C}$ values are indicated by superscript letters:

^aninhydrin;

^bEA/IRMS.

TABLE 2 Comparison of molecule-average isotopic offsets between serine standards, recovered by EA/IRMS, GC/IRMS, and GC/Orbitrap

Instrument	Analyte	$\delta^{13}\text{C}_{\text{VPDB}}$ (‰)	^{13}R	$^{13}\text{R}_{\text{normalized}}$ ^a	<i>n</i>	$\delta^{13}\text{C}_{\text{LotBCB}}$ (‰)	Added C atoms	Derivative correction factor	Serine molecule-average $\delta^{13}\text{C}_{\text{LotBCB}}$ (‰)
EA/IRMS	Lot110	-7.24 ± 0.19	0.011102 ± 2 × 10 ⁻⁶	0.011102	3	25.5 ± 0.4	0	n/a	25.5 ± 0.4
	LotBCB	-31.89 ± 0.05	0.010826 ± 3 × 10 ⁻⁶	0.010826	3				
GC/IRMS	Lot110	-28.15 ± 0.11	0.010868 ± 3 × 10 ⁻⁶	0.010868	5	9.9 ± 0.5	5	8/3	26.4 ± 1.2
	LotBCB	-37.69 ± 0.09	0.010761 ± 4 × 10 ⁻⁶	0.010761	5				
GC/Orbitrap	Lot110	n/a	0.054693 ± 6 × 10 ⁻⁵	0.010939	3	15.6 ± 1.8	2	5/3	25 ± 2
	LotBCB		0.053852 ± 7 × 10 ⁻⁵	0.010770	2				

^aThe isotope ratio from each measurement technique is divided by the number of carbon atoms in the analyte (one for the combustion product CO₂ in IRMS, versus five for the 165 Da fragment measured on the Orbitrap).

expressed relative to LotBCB. This result implies the molecular-average (C-1 + C-2 + C-3) value of $\delta^{13}\text{C}_{\text{LotBCB}} = 25 \pm 2\%$, assuming all of the difference between Lot110 and LotBCB reflects the three serine-derived atoms. Using similar logic and correcting for five reagent-derived atoms, the analogous result for GC/IRMS was 26.4 ± 1.2‰ (Table 2; Section S4, supporting information). No correction was required for the EA/IRMS result (25.5 ± 0.4‰). Thus, a comparison of all three measurements indicates that the Orbitrap measurements are in excellent agreement with those from other instruments that are well established for isotopic analysis of amino acids. Collectively, these studies verify that the measurement and

subsequent data handling accurately recover isotopic differences between analytes and standards.

We also assessed the long-term repeatability of our measurement approach in two ways. First, we examined replicate analyses of the SERCO standard over a ten-day period under typical run conditions and interspersed between plant samples. Instrument parameters were frequently re-tuned and re-calibrated during this time. Despite these potential sources of variability, average ^{13}R values were characterized with relative standard errors of 0.5‰ for the 165 Da fragment (*n* = 37), 0.3‰ for the 138 Da fragment (*n* = 8), and 0.6‰ for the 110 Da fragment (*n* = 7; Figure S3, supporting information). Second,

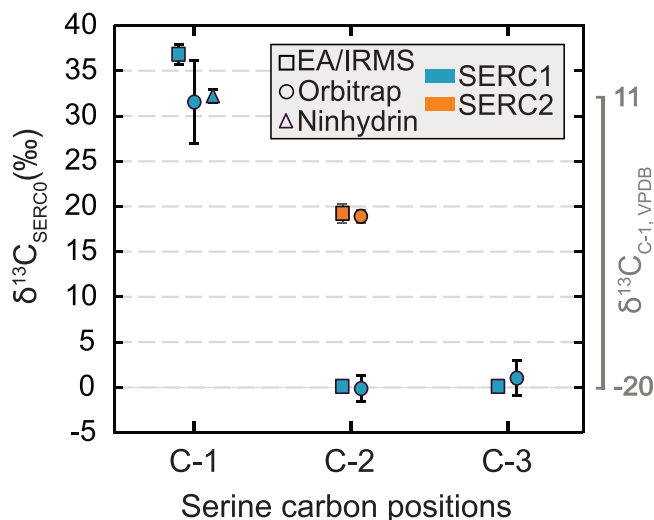


FIGURE 5 Isotopic characterization of positionally labeled serine standards by GC/Orbitrap, compared to independent constraints. Position-specific carbon isotope ratios of serine labeled at the C-1 carbon position (SERC1) or the C-2 carbon position (SERC2) are reported as $\delta^{13}\text{C}$ values (± 1 SE) relative to an unlabeled (SERC0) standard. Orbitrap results (circles) are compared to values calculated from EA/IRMS analyses of the intact molecules (squares), and to measured values for the C-1 position (liberated by reaction with ninhydrin and characterized directly by IRMS; triangle). Error bars represent the standard error of replicate measurements (± 1 SE; Table 1). The ninhydrin results for C-1 of SERC1 and SERC0 correspond to $11.2 \pm 0.5\text{‰}$ and $-20.3 \pm 0.5\text{‰}$ on the VPDB scale (right-hand axis), while the C-2 and C-3 positions are unknown on the international scale. See the supporting information for additional calculation details [Color figure can be viewed at wileyonlinelibrary.com]

we examined the full experimental reproducibility from measurement session to session for biological replicates of *Arabidopsis* plant samples. These samples were separately hydrolyzed, extracted and desalted, derivatized, and analyzed months apart under different instrument conditions and run parameters. Results from these different instrument sessions agreed within 1 or 2 SE for all fragments and position-specific $\delta^{13}\text{C}_{\text{SERC0}}$ values (Figure S4, supporting information), indicating that the method is reproducible along the entire preparatory and analytical pipeline.

3.3 | Isotopic analysis of plant samples by GC/Orbitrap

Derivatized hydrolysates of *Arabidopsis thaliana*, cultivated under different partial pressures of carbon dioxide ($p\text{CO}_2$), were characterized by GC/Orbitrap mass spectrometry. Isotope ratio measurements of serine isolated from the plant matrices revealed statistically significant differences in isotopic content among measured fragment ions (Figure 6A; Table S3) and calculated carbon positions (Figures 6B and 6C; Table S3). The largest isotopic differences between samples were measured for the 165 Da

fragment, which inherits all three carbon positions in serine and two atoms added during derivatization; the 138 Da fragment (containing C-2, C-3, and two derivative atoms) displayed the least variation across samples and no clear dependence on $p\text{CO}_2$. Calculated position-specific isotope ratios further illuminated differences among samples. The C-1 position of serine displayed the largest variation, with $\delta^{13}\text{C}_{\text{C-1,SERC0}}$ values increasing by *ca* 28‰, from $-41 \pm 2\text{‰}$ in the highest $p\text{CO}_2$ sample to $-13 \pm 5\text{‰}$ in the lowest $p\text{CO}_2$ sample. Note that these $\delta^{13}\text{C}$ values are all reported relative to our laboratory working standard, SERC0, rather than to the more common VPDB reference frame. The C-2 position also displayed a robust trend with $p\text{CO}_2$, decreasing by *ca* 13‰ from elevated to subambient $p\text{CO}_2$. Serine's C-3 position revealed the least variation and overlapping error bars for the two lower $p\text{CO}_2$ conditions (within 1 SE). Propagated errors for each carbon position are highly correlated with one another because the functions used to calculate these errors are interdependent (Equations 9-11) and cannot provide a full picture of sample resolution by this measurement. We therefore also depicted the position-specific $\delta^{13}\text{C}_{\text{SERC0}}$ values in a three-dimensional composition space, with error ellipsoids defining the 68% confidence region for each sample (Figure 6C; Figure S5, supporting information). A Monte Carlo simulation suggests that adding a fourth measurement constraint, e.g. the molecular-average $\delta^{13}\text{C}$ value characterized by GC/IRMS, could improve the precision on the C-1 position by up to 2‰.

Each plant sample acquisition was referenced to an acquisition of the SERC0 working standard, characterized shortly before or after the sample, and using all the same run parameters. The biosynthetic details for the serine stock used to develop this standard were proprietary, and the intramolecular distribution of isotopes unknown. Thus, it is important to emphasize that differences in isotopic compositions across plant samples were evaluated in a relative sense in this study. However, the C-1 isotopic composition of SERC0 was coarsely constrained to be $-20.3 \pm 0.3\text{‰}$ (SE; $n = 3$) on the VPDB scale using a degradative technique (Section 2.7; Table 1; 76% reaction yield). This result implies that the C-1 positions of *Arabidopsis* serine ranged from approximately -60.3‰ (2255 ppmv CO_2) to -33.2‰ (322 ppmv) on the VPDB scale. The strongly negative absolute values of $\delta^{13}\text{C}_{\text{C-1,VPDB}}$ partially reflect the influence of the cylinder CO_2 used to adjust the ambient $p\text{CO}_2$ levels during plant growth, as well as differences in fractionation accompanying photosynthetic CO_2 fixation under different $p\text{CO}_2$ (ϵ_P or Δ).⁵² Growth chamber CO_2 had $\delta^{13}\text{C}_{\text{VPDB}}$ values of -17.1‰ (2255 ppmv), -13.6‰ (733 ppmv), and -19.1‰ (322 ppmv), resulting in average, above-ground plant tissue $\delta^{13}\text{C}_{\text{VPDB}}$ values of -42.3‰ , -37.2‰ , and -41.4‰ , respectively.^{34,35}

3.4 | Position-specific isotopic proxies for plant serine metabolism

Based on known biochemistry, we hypothesized that isotope effects in plant metabolism would lead to measurable position-specific

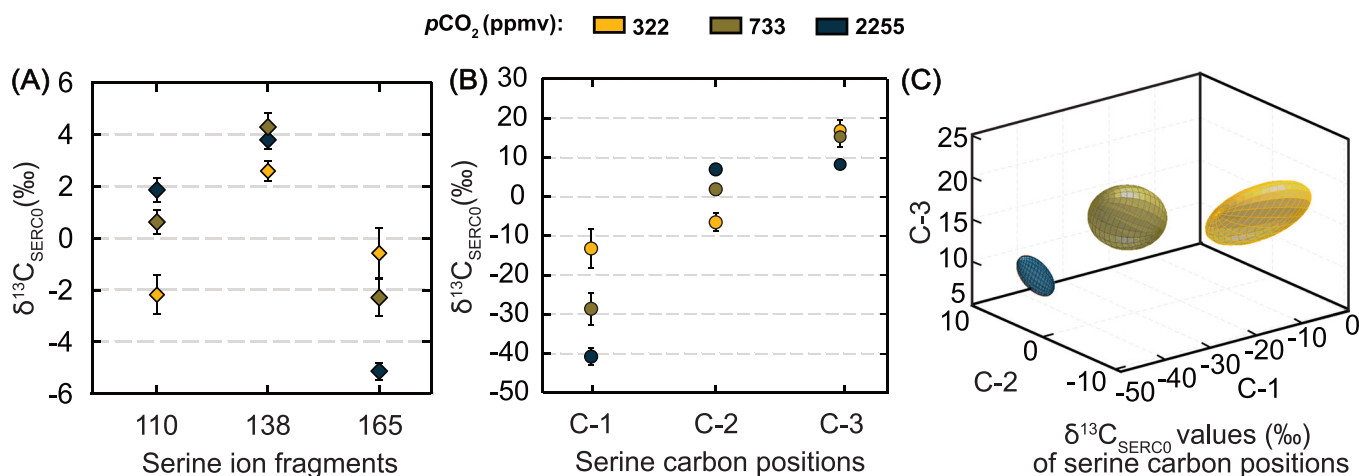


FIGURE 6 Position-specific carbon isotopic compositions of serine isolated from *Arabidopsis* biomass grown under atmospheres containing 322–2255 ppmv CO_2 . (A) $\delta^{13}\text{C}_{\text{SERCO}}$ values (± 1 SE) of serine fragments with monoisotopic masses of approximately 110, 138, or 165 Da. (B) $\delta^{13}\text{C}_{\text{SERCO}}$ values (\pm propagated 1 SE) of carbon positions in serine, calculated from fragment $\delta^{13}\text{C}$ values. Error bars not seen are within the area of the data symbols. (C) $\delta^{13}\text{C}$ values of serine carbon positions represented in three dimensions to show covariance between positions, with ellipsoids defining the 68% confidence region. Additional rotated views are shown in Figure S5 (supporting information) [Color figure can be viewed at wileyonlinelibrary.com]

differences in serine that could potentially serve as a proxy. Serine from whole leaf protein digests monitors the relative influence of three metabolic sources of serine with different biosynthetic precursors³² and predicted isotope effects.^{18,28,53,54} Metabolic precursors of serine include photorespiratory glycine and 3-phosphoglycerate, an intermediate of the Calvin cycle (i.e. photosynthesis) and glycolysis (Figure 1).

We selected plant samples grown under contrasting $p\text{CO}_2$ atmospheres to promote different balances of photorespiration (O_2 fixation) and photosynthesis (CO_2 fixation) and examine the intramolecular isotopic consequences. Although fluxes were not directly quantified by a complementary measurement technique in this study, elevated $p\text{CO}_2$ tends to suppress photorespiratory fluxes relative to photosynthesis, while subambient $p\text{CO}_2$ generally promotes photorespiration in C_3 plants.⁵⁵ Additionally, elevating $p\text{CO}_2$ can promote greater expression of the kinetic isotope effect (KIE) accompanying CO_2 fixation by RubisCO and a larger net photosynthetic carbon isotope fractionation (ϵ_P or Δ).⁵²

The strong ^{13}C enrichment we observed at serine's C-1 position with decreasing $p\text{CO}_2$ (Figure 6B) may reflect changes in both photosynthesis and photorespiration. A smaller isotopic fractionation between bulk leaf tissue and source CO_2 was observed under lower CO_2 levels (ϵ_P decreased by ca 3‰), suggesting that more CO_2 from the available pool was used under the lower $p\text{CO}_2$ conditions. Changes in photosynthetic carbon isotope fractionation would most directly impact the C-1 position of serine through the photosynthetic incorporation of CO_2 into 3-phosphoglyceraldehyde (see shading in Figure 1C). The increase in $\delta^{13}\text{C}_{\text{C-1,SERCO}}$ values with decreasing $p\text{CO}_2$ may also reflect proportionally more of the plant's serine pool originating along the photorespiratory pathway as opposed to other serine synthesis pathways. A large ^{13}C KIE of ca 22–23‰ has been

predicted for GDC based on theoretical considerations^{28,53} and of up to ca 38‰ based on modeling of multi-species leaf-level isotopic measurements.³⁵ The KIE would tend to enrich in ^{13}C both carbon positions in the residual glycine pool, which ultimately become C-1 and C-2 of serine – consistent with the enrichment we observe at C-1 (but not C-2) under lower $p\text{CO}_2$ (Figure 6B). The smaller change at C-2 in the opposite direction (Figure 6B) suggests a more significant role for the glycerate and phosphorylated pathways in explaining this position. The only reactions involving bonds to carbon in the glycerate and phosphorylated pathways are reactions at C-2: when 3-phosphoglycerate is converted to 3-phosphohydroxypyruvate (Figure 1C), or when glycerate is converted to hydroxypyruvate (Figure 1B), there is a change in the geometry around the C-2 atom from tetrahedral (sp^3) to trigonal-planar (sp^2), followed by transamination at C-2 (Figure 1). Although the isotope effects associated with these pathways have not been reported, the equilibrium isotope fractionation between serine's C-2 position and the corresponding position of its alpha-ketoacid transamination complement may be up to ca 9‰, by analogy with *ab initio* calculations for alanine.¹⁸

The isotopic contrast between the C-2 and C-3 positions for each sample (i.e. $\epsilon_{\text{C3-C2}} \approx \delta^{13}\text{C}_{\text{C3,SERCO}} - \delta^{13}\text{C}_{\text{C2,SERCO}}$) varies by approximately 19‰ across conditions, from a large contrast of 23 ± 4 ‰ in the subambient $p\text{CO}_2$ samples to a minimal contrast of 4 ± 3 ‰ in the highly elevated $p\text{CO}_2$ samples. Thus, the difference between the C-2 and C-3 positions carries an even larger signal in these experiments relative to their associated measurement errors. A potential mechanistic correspondence between the observed signature at C-3 and serine's metabolic origins is less clear. The large KIE associated with GDC would be predicted to discriminate against ^{13}C at the C-2 position of glycine that is ultimately incorporated into

the C-3 position of photorespiratory serine from methylene-THF without additional fractionation (Figure 1A).⁵⁴ Instead, in the lower $p\text{CO}_2$ experiments where we would predict more serine would originate along the photorespiratory pathway, the C-3 position of the serine pool is slightly enriched in ^{13}C when compared to the highest $p\text{CO}_2$ experiment.

We propose that further study of natural-abundance, position-specific isotope patterns within serine isolated from plants may confirm a useful signature of metabolic fluxes – including photorespiration – that could be developed into new, position-specific isotopic proxies. Plant leaves could be harvested in the field and brought back for later analysis, improving the ability to characterize such processes in non-model species growing under a wide range of environmental conditions. Additional advantages of a natural-abundance isotopic proxy include the ability to bypass the need for expensive isotope labels and the potential to integrate spatial or temporal heterogeneity of metabolic processes in individual plants or ecosystems. However, it will be important to first examine how this signature manifests in different plant species, environmental conditions (especially different temperature and humidity conditions), and at even lower $p\text{CO}_2$ levels. Proxies should be calibrated through studies using complementary quantitative measurements of photosynthetic and photorespiratory fluxes.^{56,57} A comparison of intramolecular patterns in serine from protein digests with metabolic (free) serine isolated from plants at high rates of photorespiration would provide an additional avenue for interpreting the relative importance of photorespiration versus other metabolic processes reflected in protein-bound serine in future experiments. Additionally, intramolecular measurements of serine from C_4 plants may help to constrain the non-photorespiratory endmember and further interrogate the mechanistic basis underlying these signatures.

We anticipate that our Orbitrap-based measurement approach holds additional potential for experimentally refining isotopic fractionation factors associated with photorespiration (f and g) used in models of net photosynthetic carbon isotope fractionation.^{52,53} These represent important sources of uncertainty for established paleo-environmental isotopic proxies based on fossil plant biomass.^{35,58} Moreover, this technique could probe serine metabolism in biomass more generally, e.g. microbial metabolism in environmental samples or serine's important role in one-carbon metabolism.³¹

3.5 | Outlook for Orbitrap-based amino acid PSIA

Our approach enables on-line isolation of serine from a mixture of amino acids, as well as characterization of $\delta^{13}\text{C}$ values for each carbon position in serine relative to a working standard. This work represents some of the first Orbitrap-based measurements of position-specific isotope contrasts in amino acids isolated from a biological matrix. The analytical scheme presented in this work (Section 2.1, Figure 2) should be broadly applicable to other amino acids. A variety of other proteinogenic amino acids were observed in our *Arabidopsis* samples (Figure S6, supporting information). This measurement strategy is

likely to translate to other amino acids and plant matrices with only minor modifications, e.g. to improve the hydrolysis yields and chromatographic separation of other potential analytes. We note, however, that not all amino acids are as abundant as serine or preserved during acid hydrolysis, and that analyte fragmentation does not always include breakage of every bond. There are sometimes two or more carbon positions that are not measured separately and therefore cannot be constrained using the presented approach. Conversely, fragments may form inefficiently yielding very low signal intensities, or have molecular masses that are too small to be detectable (<50 Da on the Q Exactive platform – although lower masses may be accessed through specialized tuning conditions). Luckily, EI fragment ion spectra for other trifluoroacetylated amino acids in this study and others (e.g. Jones⁵⁹) suggest that these derivatives produce a variety of prominent fragment ions that may be productive targets for PSIA of other amino acid analytes. Furthermore, alternative, established derivatization strategies (e.g. Corr et al⁴²) and/or additional fragmentation in the higher-energy collisional dissociation cell of the Q Exactive instruments may eliminate these potential obstacles for other amino acids.

Additional considerations relevant to this approach include the lack of a simple method for standardizing position-specific isotope ratio measurements for every carbon position to the international scale. Characterization of working standards by isotopic NMR provides a potential route forward, but has not yet been extended to all amino acids with sufficient precision for interlaboratory comparison. Creative or complementary standardization approaches represent important areas for future innovation. Additionally, while the presented method is substantially faster and recovers more carbon positions than existing approaches that have been applied to complex matrices, Orbitrap PSIA is nonetheless slow. The current study required *ca* 18 h per sample for triplicate sample–standard analysis. In principle, one can alternate between two or more mass windows over the course of a run using a scan event sequence within the instrument software. This modified experimental design may provide an avenue for faster sample screening or isotopic fingerprinting studies.

Looking forward, a related instrument, the Q Exactive HF with an electrospray ionization source, is highly promising for isotope ratio analysis and has been studied in detail for other analytes including pure methionine, acetate, and inorganic ions.^{14,60–62} The greatest challenge for amino acid isotope analysis by this method is the lack of efficient fragmentation (e.g. for underivatized serine, the bond between C-2 and C-3 of serine does not fracture during electrospray ionization). Nonetheless, by developing strategies to enhance fragmentation on these platforms, and by coupling these platforms to liquid chromatographic isolation of amino acids, the ESI-Orbitrap may provide an avenue to greatly increased analysis speed, even higher precision measurements, and/or elimination of the need for derivatization. Other improvements in processing transients or Orbitrap design^{45,63} could also potentially advance PSIA of natural organic materials but will require analogous, systematic study and evaluation of analytical tradeoffs.

4 | CONCLUSIONS

Intramolecular carbon isotope ordering in amino acids and other organic biomolecules is essentially unstudied for biogeochemical and ecological applications. These natural variations represent ample, underexplored opportunities to develop proxies for environmental and physiological histories. We anticipate that a method for characterizing intramolecular isotopic signatures of biomolecules like amino acids could complement the use of expensive isotope labels in metabolomics studies, and naturally trace organism-level metabolic fluxes and their interplay with the environment.

In this work, we have demonstrated that GC Orbitrap mass spectrometry can be used to extract intramolecular isotopic information about all three carbon positions of serine without requiring offline pre-purification or degradation steps. Method optimization led to experimental precisions of $\leq 1\%$ for fragments of serine from plant samples, and propagated, position-specific precisions of 0.7–5%. Through cross-platform verification with standards of distinct isotopic compositions, we validated the accuracy of our method. These are the first Orbitrap-based measurements of natural-abundance, position-specific isotope ratios in amino acids isolated from a biological matrix (plant tissues). The method is more sensitive than isotopic ^{13}C NMR by over six orders of magnitude, and isotope ratios are characterized with propagated errors that are sufficiently small to resolve differences in isotopic composition among terrestrial, natural samples. In particular, we identify intramolecular isotopic differences of up to *ca* 28‰ that may reflect relative fluxes through photorespiratory metabolism and other serine biosynthetic pathways. These measurements are encouraging for the development of isotopic proxies for plant metabolic processes, and for extension of Orbitrap PSIA to other amino acids – expanding and extending the utility of amino acid stable isotope analysis.

ACKNOWLEDGMENTS

This work was supported in part by grants from the Agouron Institute (grant number AI-F-GB54.19.2 to E.B.W.); the Center for Environmental and Microbial Interactions (to E.B.W., A.L.S., and J.M.E.); NASA Astrobiology Institute (grant number 80NSSC18M094 to A.L.S. and J.M.E.); NSF Geobiology (grant number EAR-1921330 to A.L.S.); the Simons Foundation (to J.M.E.); DOE (award number DE-SC0016561 to J.M.E.); and the Research Council of Norway (funding scheme number 223272 to A.H.J.). The authors thank Hanako Yoshiro and Elliott Meyerowitz for furnishing *A. thaliana* seedlings and cultivation supplies during method development, Alexis Gilbert for performing the ninhydrin reaction of serine standards at Tokyo Tech, and Nami Kitchen and Fenfang Wu for laboratory support. This work benefited from helpful discussions about method development and data processing with Guannan Dong, Elliott Mueller, Laura Chimiak, Tim Csernica, Max Lloyd, Gabriella Weiss, Kate Freeman, Alexandra Phillips, and Caj Neubauer. The authors thank Roland Bol for editorial handling and two anonymous reviewers for their valuable comments.

PEER REVIEW

The peer review history for this article is available at <https://publons.com/publon/10.1002/rcm.9347>.

DATA AVAILABILITY STATEMENT

Data available on request from the authors.

ORCID

Elise B. Wilkes  <https://orcid.org/0000-0002-3379-7832>

Alex L. Sessions  <https://orcid.org/0000-0001-6120-2763>

Sarah S. Zeichner  <https://orcid.org/0000-0001-8897-7657>

Brooke Dallas  <https://orcid.org/0000-0002-1313-3270>

A. Hope Jahren  <https://orcid.org/0000-0003-3884-1676>

REFERENCES

- Larsen T, Taylor D, Leigh MB, OBrien DM. Stable isotope fingerprinting: A novel method for identifying plant, fungal or bacterial origins of amino acids. *Ecology*. 2009;90(12):3526-3535. doi:[10.1890/08-1695.1](https://doi.org/10.1890/08-1695.1)
- Larsen T, Ventura M, Andersen N, OBrien DM, Piatkowski U, McCarthy MD. Tracing carbon sources through aquatic and terrestrial food webs using amino acid stable isotope fingerprinting. *PLoS ONE*. 2013;8(9):e73441. doi:[10.1371/journal.pone.0073441](https://doi.org/10.1371/journal.pone.0073441)
- McMahon KW, Fogel ML, Elsdon TS, Thorrold SR. Carbon isotope fractionation of amino acids in fish muscle reflects biosynthesis and isotopic routing from dietary protein. *J Anim Ecol*. 2010;79(5):1132-1141. doi:[10.1111/j.1365-2656.2010.01722.x](https://doi.org/10.1111/j.1365-2656.2010.01722.x)
- Scott JH, OBrien DM, Emerson D, Sun H, McDonald GD, et al. An examination of the carbon isotope effects associated with amino acid biosynthesis. *Astrobiology*. 2006;6(6):867-880. doi:[10.1089/ast.2006.6.867](https://doi.org/10.1089/ast.2006.6.867)
- Whiteman JP, Smith EA, Besser AC, Newsome SD. A guide to using compound-specific stable isotope analysis to study the fates of molecules in organisms and ecosystems. *Diversity*. 2019;11(1):8. doi:[10.3390/d11010008](https://doi.org/10.3390/d11010008)
- Brenna JT. Natural intramolecular isotope measurements in physiology: Elements of the case for an effort toward high-precision position-specific isotope analysis. *Rapid Commun Mass Spectrom*. 2001;15(15):1252-1262. doi:[10.1002/rcm.325](https://doi.org/10.1002/rcm.325)
- Hayes JM. Fractionation of the isotopes of carbon and hydrogen in biosynthetic processes. In: *Reviews in Mineralogy and Geochemistry* 43, *Stable Isotope Geochemistry*. Washington, DC: Mineralogical Society of America. 2001;1:225-277. doi:[10.2138/gsmg.43.1.225](https://doi.org/10.2138/gsmg.43.1.225)
- Rossmann A, Butzenlechner M, Schmidt H-L. Evidence for a nonstatistical carbon isotope distribution in natural glucose. *Plant Physiol*. 1991;96(2):609-614. doi:[10.1104/pp.96.2.609](https://doi.org/10.1104/pp.96.2.609)
- Schmidt H-L. Fundamentals and systematics of the non-statistical distributions of isotopes in natural compounds. *Naturwissenschaften*. 2003;90(12):537-552. doi:[10.1007/s00114-003-0485-5](https://doi.org/10.1007/s00114-003-0485-5)
- Abelson PH, Hoering TC. Carbon isotope fractionation in formation of amino acids by photosynthetic organisms. *Proc Natl Acad Sci USA*. 1961;47:623-632. doi:[10.1073/pnas.47.5.623](https://doi.org/10.1073/pnas.47.5.623)
- Chimiak L, Elsilä JE, Dallas B, et al. Carbon isotope evidence for the substrates and mechanisms of prebiotic synthesis in the early solar system. *Geochim Cosmochim Acta*. 2021;292:188-202. doi:[10.1016/j.gca.2020.09.026](https://doi.org/10.1016/j.gca.2020.09.026)
- Fry B, Carter JF, Yamada K, Yoshida N, Juchelka D. Position-specific $^{13}\text{C}/^{12}\text{C}$ analysis of amino acid carboxyl groups: Automated flow-injection analysis based on reaction with ninhydrin. *Rapid Commun Mass Spectrom*. 2018;32(12):992-1000. doi:[10.1002/rcm.8126](https://doi.org/10.1002/rcm.8126)
- Fry B, Carter JF. Stable carbon isotope diagnostics of mammalian metabolism, a high-resolution isotomics approach using amino acid

- carboxyl groups. *PLoS One*. 2019;14(10):e0224297. doi:10.1371/journal.pone.0224297
14. Neubauer C, Sweredoski MJ, Moradian A, Newman DK, Robins RJ, Eiler JM. Scanning the isotopic structure of molecules by tandem mass spectrometry. *Int J Mass Spectrom*. 2018;434:276-286. doi:10.1016/j.ijms.2018.08.001
 15. Rasmussen C, Hoffman DW. Intramolecular distribution of $^{13}\text{C}/^{12}\text{C}$ isotopes in amino acids of diverse origins. *Amino Acids*. 2020;52(6-7):955-964. doi:10.1007/s00726-020-02863-y
 16. Savidge WB, Blair NE. Seasonal and within-plant gradients in the intramolecular carbon isotopic composition of amino acids of *Spartina alterniflora*. *J Exp Mar Bio Ecol*. 2004a;308(2):151-167. doi:10.1016/j.jembe.2004.02.010
 17. Savidge WB, Blair NE. Patterns of intramolecular carbon isotopic heterogeneity within amino acids of autotrophs and heterotrophs. *Oecologia*. 2004;139(2):178-189. doi:10.1007/s00442-004-1500-z
 18. McNeill AS, Dallas BH, Eiler JM, Bylaska EJ, Dixon DA. Reaction energetics and ^{13}C fractionation of alanine transamination in the aqueous and gas phases. *J Phys Chem A*. 2020;124(10):2077-2089. doi:10.1021/acs.jpca.9b11783
 19. Rustad JR. Ab initio calculation of the carbon isotope signatures of amino acids. *Org Geochem*. 2009;40(6):720-723. doi:10.1016/j.orggeochem.2009.03.003
 20. Gauchotte-Lindsay C, Turnbull SM. On-line high-precision carbon position-specific stable isotope analysis: A review. *Trends Anal Chem*. 2016;76:115-125. doi:10.1016/j.trac.2015.07.010
 21. Gilbert A. The organic isotopologue frontier. *Annu Rev Earth Planet Sci*. 2021;49(1):435-464. doi:10.1146/annurev-earth-071420-053134
 22. Jézéquel T, Joubert V, Giraudeau P, Remaud GS, Akoka S. The new face of isotopic NMR at natural abundance. *Magn Reson Chem*. 2017;55(2):77-90. doi:10.1002/mrc.4548
 23. Romek KM, Krzeminska A, Remaud GS, Julien M, Paneth P, Robins RJ. Insights into the role of methionine synthase in the universal ^{13}C depletion in O- and N-methyl groups of natural products. *Arch Biochem Biophys*. 2017;635:60-65. doi:10.1016/j.abb.2017.10.012
 24. Hayes JM. Practice and Principles of Isotopic Measurements in Organic Geochemistry. 2002. <https://www.whoi.edu/files/server.do?id=73290&pt=2&p=74886>
 25. Dallas BH, Eiler JM, Chimiak LM, Sessions AL. Position-specific carbon isotope measurements in alanine by high-resolution gas-source IRMS. *Goldschmidt Abstracts*. 2017:822.
 26. Eiler J, Cesar J, Chimiak L, et al. Analysis of molecular isotopic structures at high precision and accuracy by Orbitrap mass spectrometry. *Int J Mass Spectrom*. 2017;422:126-142. doi:10.1016/j.ijms.2017.10.002
 27. Phillips A, Wu F, Sessions A. Sulfur isotope analysis of cysteine and methionine via preparatory liquid chromatography and elemental analyzer isotope ratio mass spectrometry. *Rapid Commun Mass Spectrom*. 2021;35(4):e9007. doi:10.1002/rcm.9007
 28. Tcherkez G. How large is the carbon isotope fractionation of the photorespiratory enzyme glycine decarboxylase? *Funct Plant Biol*. 2006;33(10):911-920. doi:10.1071/FP06098
 29. Ho C-L, Saito K. Molecular biology of the plastidic phosphorylated serine biosynthesis pathway in *Arabidopsis thaliana*. *Amino Acids*. 2001;20(3):243-259. doi:10.1007/s007260170042
 30. Igamberdiev AU, Kleczkowski LA. The glycerate and phosphorylated pathways of serine synthesis in plants: The branches of plant glycolysis linking carbon and nitrogen metabolism. *Front Plant Sci*. 2018;9:318. doi:10.3389/fpls.2018.00318
 31. Li R, Moore M, King J. Investigating the regulation of one-carbon metabolism in *Arabidopsis thaliana*. *Plant Cell Physiol*. 2003;44(3):233-241. doi:10.1093/pcp/pcg029
 32. Ros R, Muñoz-Bertomeu J, Krueger S. Serine in plants: Biosynthesis, metabolism, and functions. *Trends Plant Sci*. 2014;19(9):564-569. doi:10.1016/j.tplants.2014.06.003
 33. VanSlyke DD, Dillon RT, MacFayden DA, Hamilton P. Gasometric determination of carboxyl groups in free amino acids. *J Biol Chem*. 1941;141(2):627-669. doi:10.1016/S0021-9258(18)72810-X
 34. Schubert BA, Jahren AH. The effect of atmospheric CO_2 concentration on carbon isotope fractionation in C_3 land plants. *Geochim Cosmochim Acta*. 2012;96:29-43. doi:10.1016/j.gca.2012.08.003
 35. Schubert BA, Jahren AH. Incorporating the effects of photorespiration into terrestrial paleoclimate reconstruction. *Earth Sci Rev*. 2018;177:637-642. doi:10.1016/j.earscirev.2017.12.008
 36. Hagopian WM, Schubert BA, Jahren AH. Large-scale plant growth chamber design for elevated pCO_2 and $\delta^{13}\text{C}$ studies. *Rapid Commun Mass Spectrom*. 2015;29(5):440-446. doi:10.1002/rcm.7121
 37. Hagopian WM, Schubert BA, Graper RA, Jahren AH. Plant growth chamber design for subambient pCO_2 and $\delta^{13}\text{C}$ studies. *Rapid Commun Mass Spectrom*. 2018;32(15):1296-1302. doi:10.1002/rcm.8176
 38. Silverman SN, Phillips AA, Weiss GM, Wilkes EB, Eiler JM, Sessions AL. Practical considerations for amino acid isotope analysis. *Org Geochem*. 2022;164:104345. doi:10.1016/j.orggeochem.2021.104345
 39. Jim S, Jones V, Copley MS, Ambrose SH, Evershed RP. Effects of hydrolysis on the $\delta^{13}\text{C}$ values of individual amino acids derived from polypeptides and proteins. *Rapid Commun Mass Spectrom*. 2003;17(20):2283-2289. doi:10.1002/rcm.1177
 40. Metges CC, Daenzer M. ^{13}C gas chromatography-combustion isotope ratio mass spectrometry analysis of N-pivaloyl amino acid esters of tissue and plasma samples. *Anal Biochem*. 2000;278(2):156-164. doi:10.1006/abio.1999.4426
 41. Takano Y, Kashiyama Y, Ogawa NO, Chikaraishi Y, Ohkouchi N. Isolation and desalting with cation-exchange chromatography for compound-specific nitrogen isotope analysis of amino acids: Application to biogeochemical samples. *Rapid Commun Mass Spectrom*. 2010;24(16):2317-2323. doi:10.1002/rcm.4651
 42. Corr LT, Berstan R, Evershed RP. Optimisation of derivatisation procedures for the determination of $\delta^{13}\text{C}$ values of amino acids by gas chromatography/combustion/isotope ratio mass spectrometry. *Rapid Commun Mass Spectrom*. 2007;21(23):3759-3771. doi:10.1002/rcm.3252
 43. Zeichner SS, Wilkes EB, Hofmann AE, et al. Methods and limitations of stable isotope measurements via direct elution of chromatographic peaks using gas chromatography-Orbitrap mass spectrometry. *Int J Mass Spectrom*. 2022;477:116848. doi:10.1016/j.ijms.2022.116848
 44. Makarov A. Electrostatic axially harmonic orbital trapping: A high-performance technique of mass analysis. *Anal Chem*. 2000;72(6):1156-1162. doi:10.1021/ac991131p
 45. Bills JR, Nagornov KO, Kozhinov AN, Williams TJ, Tsybin YO, Marcus RK. Improved uranium isotope ratio analysis in liquid sampling-atmospheric pressure glow discharge/Orbitrap FTMS coupling through the use of an external data acquisition system. *J Am Soc Mass Spectrom*. 2021;32(5):1224-1236. doi:10.1021/jasms.1c00051
 46. Scigelova M, Hornshaw M, Giannakopoulos A, Makarov A. Fourier transform mass spectrometry. *Mol Cell Proteomics*. 2011;10(7):M111, 009431. doi:10.1074/mcp.M111.009431
 47. Rieley G. Derivatization of organic compounds prior to gas chromatographic combustion-isotope ratio mass spectrometric analysis: Identification of isotope fractionation processes. *Analyst*. 1994;119(5):915-919. doi:10.1039/AN9941900915
 48. Gorshkov MV, Fornelli L, Tsybin YO. Observation of ion coalescence in Orbitrap Fourier transform mass spectrometry. *Rapid Commun Mass Spectrom*. 2012;26(15):1711-1717. doi:10.1002/rcm.6289
 49. Hofmann AE, Chimiak L, Dallas B, et al. Using Orbitrap mass spectrometry to assess the isotopic compositions of individual

- compounds in mixtures. *Int J Mass Spectrom.* 2020;457:116410 doi: [10.1016/j.ijms.2020.116410](https://doi.org/10.1016/j.ijms.2020.116410)
50. Matucha M, Jockisch W, Verner P, Anders G. Isotope effect in gas-liquid chromatography of labelled compounds. *J Chromatogr A.* 1991; 588(1-2):251-258. doi: [10.1016/0021-9673\(91\)85030-J](https://doi.org/10.1016/0021-9673(91)85030-J)
51. Chimiak L. *Prebiotic fingerprints*. PhD dissertation. California Institute of Technology; 2021. doi: [10.7907/Ohvh-xz81](https://doi.org/10.7907/Ohvh-xz81)
52. Farquhar GD, OLeary MH, Berry JA. On the relationship between carbon isotope discrimination and the intercellular carbon dioxide concentration in leaves. *J Plant Physiol.* 1982;9(2):121-137. doi: [10.1017/PP9820121](https://doi.org/10.1017/PP9820121)
53. Lanigan GJ, Betson N, Griffiths H, Seibt U. Carbon isotope fractionation during photorespiration and carboxylation in *Senecio*. *Plant Physiol.* 2008;148(4):2013-2020. doi: [10.1104/pp.108.130153](https://doi.org/10.1104/pp.108.130153)
54. Gleixner G. Insights into the known ¹³C depletion of methane: Contribution of the kinetic isotope effects on the serine hydroxymethyltransferase reaction. *Front Chem.* 2022;9:698067. doi: [10.3389/fchem.2021.698067](https://doi.org/10.3389/fchem.2021.698067)
55. Sharkey TD. Estimating the rate of photorespiration in leaves. *Physiol Plant.* 1988;73(1):147-152. doi: [10.1111/j.1399-3054.1988.tb09205.x](https://doi.org/10.1111/j.1399-3054.1988.tb09205.x)
56. Busch F. Current methods for estimating the rate of photorespiration in leaves. *Plant Biol.* 2013;15(4):648-655. doi: [10.1111/j.1438-8677.2012.00694.x](https://doi.org/10.1111/j.1438-8677.2012.00694.x)
57. Busch F. Photorespiration in the context of rubisco biochemistry, CO₂ diffusion and metabolism. *Plant J.* 2020;101:919-939. doi: [10.1111/tpj.14674](https://doi.org/10.1111/tpj.14674)
58. Hare VJ, Laverigne A. Differences in carbon isotope discrimination between angiosperm and gymnosperm woody plants, and their geological significance. *Geochim Cosmochim Acta.* 2021;300:215-230. doi: [10.1016/j.gca.2021.02.029](https://doi.org/10.1016/j.gca.2021.02.029)
59. Jones V. *Investigating the routing and synthesis of amino acids between diet and bone collagen via feeding experiments and applications to paleodietary reconstruction*. PhD thesis. University of Bristol; 2002.
60. Hilkert A, Böhlke JK, Mroczkowski SJ, et al. Exploring the potential of electrospray-Orbitrap for stable isotope analysis using nitrate as a model. *Anal Chem.* 2021;93(26):9139-9148. doi: [10.1021/acs.analchem.1c00944](https://doi.org/10.1021/acs.analchem.1c00944)
61. Mueller EP, Sessions AL, Sauer PE, Weiss GM, Eiler JM. Simultaneous, high-precision measurements of δ²H and δ¹³C in nanomole quantities of acetate using electrospray ionization-quadrupole-Orbitrap mass spectrometry. *Anal Chem.* 2022;94(2): 1092-1100. doi: [10.1021/acs.analchem.1c04141](https://doi.org/10.1021/acs.analchem.1c04141)
62. Neubauer C, Crémière A, Wang X, et al. Stable isotope analysis of intact oxanions using electrospray quadrupole-Orbitrap mass spectrometry. *Anal Chem.* 2021;92(4):3077-3085. doi: [10.1021/acs.analchem.9b04486](https://doi.org/10.1021/acs.analchem.9b04486)
63. Denisov E, Damoc E, Makarov A. Exploring frontiers of orbitrap performance for long transients. *Int J Mass Spectrom.* 2021;466: 116607. doi: [10.1016/j.ijms.2021.116607](https://doi.org/10.1016/j.ijms.2021.116607)

SUPPORTING INFORMATION

Additional supporting information can be found online in the Supporting Information section at the end of this article.

How to cite this article: Wilkes EB, Sessions AL, Zeichner SS, et al. Position-specific carbon isotope analysis of serine by gas chromatography/Orbitrap mass spectrometry, and an application to plant metabolism. *Rapid Commun Mass Spectrom.* 2022;36(18):e9347. doi: [10.1002/rcm.9347](https://doi.org/10.1002/rcm.9347)